Quantitative Image Features of Gadoxetic Acid–enhanced MRI for Predicting Glypican-3 Expression of Small Hepatocellular Carcinoma ≤ 3 cm

San-Yuan Dong
Fudan University
Wei Sun
Fudan University
Bin Xu
Fudan University
Wen-Tao Wang
Fudan University
Yu-Tao Yang
Fudan University
Xiao-Shan Chen
Fudan University
Meng-Su Zeng
Fudan University
Sheng-Xiang Rao (raoxray@163.com)
Fudan University https://orcid.org/0000-0003-3597-7770

Research Article

Keywords: Magnetic resonance imaging, Gd-EOB-DTPA, Liver neoplasms, Nomogram, Prognosis, Recurrence-free survival, Risk factor, AFP, Retrospective studies, Proliferation

Posted Date: July 8th, 2022

DOI: https://doi.org/10.21203/rs.3.rs-1807616/v1

Abstract

Background/purpose of the study: Glypican-3 (GPC3) is associated with the occurrence and poor prognosis of hepatocellular carcinoma (HCC). To explore the value of quantitative image features of Gadoxetic Acid–enhanced magnetic resonance imaging (MRI) for predicting GPC3 expression of single HCC ≤ 3 cm.

Methods: One hundred and forty-nine patients with pathologically confirmed HCC (training cohort: n=117; validation cohort: n=32) were included retrospectively. Quantitative image features and clinicopathological parameters were analyzed. The significant predictors for GPC3 expression were identified using multivariate logistic regression analyses. Nomograms were constructed from the prediction model and recurrence rates was evaluated by the Kaplan–Meier method.

Results: Serum alpha-fetoprotein (AFP) > 20 ng/mL (odds ratio [OR] = 5.215; p = 0.004) and tumor-to-liver signal intensity (SI) ratio on hepatobiliary phase (HBP) (OR = 0.003; p = 0.005) were independent significant factors for GPC3 expression. When these two factors were combined, the diagnostic specificity of the training cohort and validation cohort was 87.9 (29/33) and 90.0 (9/10), respectively. The nomogram based on the predictive model performed satisfactorily in the training (C-index: 0.856) and validation (C-index: 0.877) cohort. Recurrence rates were significantly higher in patients with GPC3-positive HCCs compared with those with GPC3-negative HCCs after curative resection in the training (45.9% vs. 25.0%, P=0.034) and validation (54.5% vs. 30.0%, P=0.042) cohorts.

Conclusion: Serum AFP > 20 ng/mL combined with tumor-to-liver SI ratio on HBP are potential predictive factors for GPC3 expression of HCC ≤ 3cm. GPC3-positive is correlated with a poor prognosis in HCC patients.

Lay Summary

- Serum AFP > 20 ng/mL combined with tumor-to-liver SI ratio on HBP were independent predictors for GPC3 expression of HCC.
- The combinational model prepared from the two findings satisfactorily predicted GPC3 expression, and GPC3-positive was associated with recurrence after surgical resection in HCC patients.
- This model could help clinicians in the preoperative management of small HCC ≤ 3 cm.

Introduction

Hepatocellular carcinoma (HCC) is the most common primary liver cancer and the third leading cause of cancer related death worldwide [1]. The treatment of HCC has made progress, but its prognosis is still very poor [2, 3]. Glypican-3 (GPC3), a heparin sulfate proteoglycan, is associated with HCC tumorigenesis and poor prognosis [4]. It is highly expressed in HCC patients and plays an important role in cell proliferation and differentiation, promoting the progression and metastasis of HCC patients [5, 6]. Studies have shown that GPC3 could be an immunotherapeutic target for hepatocellular carcinoma [7, 8]. Although GPC3 expression can be detected by liver biopsy before surgery, this invasive method does not reflect the heterogeneity of the entire tumor and may be unreliable due to sample variation [9]. Thus, preoperative evaluation of GPC3 expression by using noninvasive imaging techniques is helpful for diagnosis, treatment and prognosis of HCC.

Gadoxetic acid-enhanced magnetic resonance imaging (MRI) has high sensitivity in diagnosis of HCC, especially for small HCC [10, 11]. Previous studies have shown that some imaging features of HCC based on gadoxetic acid-

enhanced MRI, such as irregular tumor margin, arterial rim enhancement, and lower tumor-to-liver signal intensity (SI) ratio at hepatobiliary phase (HBP) images, can predict its biological behavior [12, 13]. However, there is no study to predict the expression of GPC3 in HCC based on these imaging features.

Three-dimensional (3D) quantitative analysis is a technique that furnishes a more detailed and repeatable quantitative assessment of the tumor characteristics, which can be used for preoperative diagnosis and risk stratification of tumors [14, 15]. A recent study has shown that the 3D quantitative analysis of gadoxetic acid-enhanced MRI can predict MVI of small HCC ≤ 3 cm [16]. We hypothesis that 3D quantitative analysis and imaging features of gadoxetic acid-enhanced MRI may help predict GPC3 of small HCC.

Therefore, the purpose of this study was to explore the significance of preoperative 3D quantitative analysis and imaging features of gadoxetic acid-enhanced MR for predicting GPC3 and the relationship between GPC3 status and recurrence after surgery of single HCC ≤ 3 cm.

Materials And Methods

The institutional review board approved this retrospective study and waived the requirement for informed consent.

Study Design

The patients were divided into the training cohort and the validation cohort according to time. The data from the training cohort enabled the screening of the significant image findings and established the GPC3 prediction model. The data from the validation cohort verified the diagnostic performance of the prediction model.

Patients

Consecutive patients who underwent gadoxetic acid-enhanced MRI before HCC resection from July 2012 to October 2019 were retrospectively included. The criteria for patient inclusion are as follows: pathologically proven single HCC without suspicious lymph nodes, longest tumor diameter ≤ 3 cm in MR imaging and have GPC3 immunochemical staining. The inclusion and exclusion criteria are summarized in the patient flow diagram shown in Fig. 1.

MR Imaging Data

All MR images were acquired using a 1.5 T scanner (MAGNETOM Aera, Siemens Healthcare) with an intravenous bolus injection of 0.025 mmol/kg gadoxetic acid (Primovist, Bayer HealthCare Pharmaceuticals Inc.). The MRI sequences included: T2-weighted phase with fat suppression, diffusion-weighted imaging (DWI), pre-contrast T1-weighted phase and post-contrast dynamic T1-weighted volumetric-interpolated breath-hold examination (VIBE) at arterial phase (20–30 seconds), portal venous phase (60–70 seconds), transitional phase (3 minutes), and HBP (20 minutes). Detailed parameters of each MRI sequence are shown in Table S1.

Imaging Analysis

The image features analyzed in this study include 3D quantification analysis, traditional quantitative and qualitative image features. MR images were independently evaluated by two radiologists (with 6 and 18 years of experience in liver MRI, respectively; hereafter referred to as reader 1 and reader 2, respectively).

3D Quantitative Analysis

Tumor segmentation was performed using the LIFEx software (http://www.lifexsoft.org). Previous studies have shown that the boundary of the lesion is best visualized in the HBP images [17]. Therefore, in this study, the region of interest (ROI) was manually segmented along the tumor boundary on the HBP image by reader 1. Next, 50 randomly selected tumors (40 in the training cohort and 10 in the validation cohort) were re-segmented by reader 2 to test the reproducibility of the features extracted from the segmentations [18]. Both readers were blinded to clinical, laboratory, histopathological, and follow-up results. The representative cases of tumor contouring on MR images are shown in Fig. 2–3.

After profiling the whole tumor, three 3D quantitative parameters were calculated by the LIFEx software: (1) Volume (mL), the volume of interest in mL; (2) Sphericity, ranging from 0 to 1. The sphericity of a perfect sphere is equal to 1; (3) Compacity, reflecting how compact the lesion is. The formulas of 3D quantitative parameter are given in Online Resource.

Traditional Imaging Features

The traditional quantitative image features included in this study are as follows: tumor size, tumor apparent diffusion coefficient (ADC) value, tumor-to-liver SI ratio on DWI, and tumor-to-liver SI ratio on HBP. Tumor size was defined as the maximum diameter on the transverse image. The other parameters were evaluated at the level of the maximum tumor diameter. Manually place the ROI on the ADC map, DWI (b value of 500 sec/mm^2) and HBP image to approximately cover the entire tumor area. The peripheral portion was excluded to prevent the interference of the partial volume effect of adjacent tissues. All lesions were first evaluated by reader 1. Then, 50 randomly selected tumors (the same as those mentioned in the 3D quantitative analysis) were re- evaluated by reader 2 to test the reproducibility of the features. Further details are given in Online Resource.

The qualitative image features were independently reviewed by the two readers using a picture archiving and communication system (PACS): (a) arterial rim enhancement, (b) arterial peritumoral enhancement, (c) tumor margin, (d) tumor capsule, (e) tumor hypointensity on HBP, (f) peritumoral hypointensity on HBP, and (g) enhancement pattern. After independent image review, interobserver agreement was evaluated. When there was a discrepancy between the two readers, a joint review was conducted to reach a consensus on the final decision. Further details are given in the supplementary material.

Histopathological Diagnosis and Follow-up

Pathologic data analyzed in our study were the GPC3 expression, presence of microvascular invasion (MVI), intrahepatic location, presence of cirrhosis, etiology of liver disease, Edmondson-Steiner grade, and presence of satellite nodule. Immunoreactivity was evaluated as the positive percent area of GPC3. To minimize false-positive interference, GPC3 expression was defined as the presence of immunoreactivity in at least 5% of tumor cells, and cases with tumor cell immunoreactivity lower than 5% were excluded. MVI was defined as the presence of tumor emboli in tiny blood vessels near the primary tumor, which was only visible under a microscope. This information comes from surgical and pathologic reports initially completed by two experienced pathologists (with 15 and 21 years of experience in liver histopathological diagnosis, respectively). After surgical resection, the patients were monitored by multi-phase liver computed tomography (CT) or MRI and serum alpha-fetoprotein (AFP) every 3–6 months to assess tumor recurrence.

Nomogram Construction and Evaluation

The nomogram was constructed according to the prediction model and illustrated in a graphical manner. Harrell's C-index assessed the discrimination performance of the nomogram. Calibration curves analyzed the diagnostic performance of the nomogram in the training and validation cohorts. The decision curve quantifies the net benefit of the entire cohort under different threshold probabilities to determine the clinical efficacy of the nomogram

Statistical Analysis

Categorical variables were analyzed using Chi-square test or Fisher's exact test. Continuous variables were analyzed using two-sample t-test or the Mann-Whitney U test. The interobserver agreement was determined using kappa statistics and intraclass correlation coefficients (ICC): poor for 0 − 0.2, fair for 0.2 − 0.4, moderate for 0.4 − 0.6, good for 0.6 − 0.8, and excellent for 0.8 − 1.0. Univariate and multivariate logistic regression were performed to assess the independent risk factors for GPC3 expression. Receiver operating characteristic (ROC) curve and area under the curve (AUC) were performed to evaluate the diagnostic performances of significant findings. The best cutoff value for ROC curve was calculated by Youden's index. Sensitivity, specificity, accuracy, positive predictive value (PPV), and negative predictive value (NPV) of significant imaging findings were also calculated. Nomograms were built based on this prediction model. The recurrence curves were estimated by the Kaplan-Meier method, and differences among the subgroups were compared by the log-rank test. Statistical analyses were performed using SPSS software (version 26.0) and R software (version 3.6.1). $P < 0.05$ was considered significant.

Results

Demographic and Pathologic Characteristics

Table 1 shows the baseline clinical and pathologic characteristics of HCC. The final cohort of 149 patients (123 men and 26 women) was classified into two cohorts. The training cohort included 117 patients (84 for GPC3-positive, 33 for GPC3-negative; 98 men and 19 women) and was conducted from July 2012 to December 2017. The time-independent validation cohort included 32 patients (22 for GPC3-positive, 10 for GPC3-negative; 25 men and 7 women) and was conducted from January 2018 to October 2019.

In the training cohort, statistical differences between the GPC3-positive and GPC3-negative patients were observed in the following characteristics: age ($P = 0.009$), Edmondson-Steiner grade ($P = 0.001$), serum AFP ($P <0.001$), and MVI ($P = 0.018$). For age, GPC3-positive patients are younger than those GPC3-negative. For serum AFP, more patients with serum AFP more than 20 ng/mL in the GPC3-positive group than in the GPC3-negative group. Edmondson-Steiner grade and MVI were postoperative features and not included in the multivariate analysis. No significant difference was observed between the training cohort and the validation cohort, including GPC3 status ($P >0.05$).

MR imaging characteristics

Table 2 shows the quantitative MR imaging features of HCC. In the training cohort, statistical differences between the GPC3-positive and GPC3-negative patients were observed in the following image features: tumor volume ($P = 0.031$), compacity ($P = 0.034$), tumor-to-liver SI ratio on DWI ($P = 0.031$), and tumor-to-liver SI ratio on HBP ($P <0.001$). The ICCs for the imaging findings were 0.936-0.998 ($P <0.001$). The tumor volume of GPC3-positive HCCs was larger than that of GPC3-negative HCCs. The tumor compacity of GPC3-positive HCCs were larger than that of GPC3-negative HCCs, suggesting the more compact nature of GPC3-positive HCC lesions. The tumor-to-liver SI ratio on DWI of GPC3-positive HCCs were larger than the respective parameters of GPC3-positive HCCs. The tumor-

to-liver SI ratio on HBP of GPC3-positive HCCs were less than the respective parameters of GPC3-positive HCCs. No statistical difference was identified in the quantitative imaging features between the training and the validation cohorts (P >0.05).

Table 3 shows the qualitative MR imaging findings of HCC. In the training cohort, no statistical difference was identified in the qualitative imaging features between the GPC3-positive and GPC3-negative patients (P >0.05). No statistical difference was identified in the qualitative imaging features between the training and the validation cohorts (P >0.05).

Prediction Model

Table 4 shows the results of the univariate and multivariate analyses of imaging findings related to GPC3 expression in the training cohort. The variables showing P <0.1 in the univariate logistic regression analyses were applied to multivariate logistic regression analysis. Statistical difference was observed in the serum AFP > 20 ng/mL (odds ratio [OR], 5.215; P = 0.004) and tumor-to-liver SI ratio on HBP (OR, 0.003; P = 0.005) finally for GPC3 expression in HCC. The optimal cutoff value of tumor-to-liver SI ratio on HBP was 0.677 according to Youden's index of the ROC.

Table 5 shows sensitivity, specificity, accuracy, PPV, and NPV for predicting GPC3 using the two significant factors and their combinations. In the training cohort, when the two factors were combined, the values for sensitivity, specificity and accuracy were 51.2(43/84), 87.9(29/33) and 61.5(72/117), respectively. In the validation cohort, when the two factors were combined, the values for sensitivity, specificity and accuracy were 50.0(11/22), 90.0(9/10) and 62.5(20/32), respectively.

The resulting AUC values of diagnostic model (with the two significant factors combined) were 0.856 (95% confidence interval [CI]: 0.782, 0.930; training cohort) and 0.877 (95% CI: 0.735, 1.000; validation cohort) (Fig. 4). The diagnostic model exhibited the highest predictive value compared to that obtained using each significant MRI finding alone.

Development and Validation of the Nomogram

The nomogram for predicting GPC3 expression using the two significant MR imaging findings is illustrated in Fig. 5. The training cohort (C-index 0.856) and the validation cohort (C-index 0.877) were predicted satisfactorily. The calibration curves for prediction and observation agreed well in both cohorts. The net benefit of the decision curve for the predictive nomogram in the whole cohort was higher than that when it was assumed that all or no patients expressed GPC3-positive. Moreover, the threshold probability was between 2% and 88%, indicating that the therapy strategy based on our nomogram would be capable of improving clinical outcomes.

Recurrence rate

The recurrence rates of patients are described in Fig. 6**.** In the training cohort, during the entire follow-up period (range, 28-1096 days; median, 844 days), the recurrence rates of the two groups patients with GPC3-positive and GPC3-negative HCCs were 45.9% (39/85) and 25.0% (8/32), respectively. In the validation cohort, during the entire follow-up period (range, 29–1237 days; median, 734 days), the recurrence rates of the two groups were 54.5% (12/22) and 30.0% (3/10), respectively. Recurrence rates were significantly higher in patients with GPC3-positive HCCs compared with those with GPC3-negative HCCs after curative resection in the training (45.9% vs. 25.0%, P = 0.034) and validation (54.5% vs. 30.0%, P = 0.042) cohorts.

Discussion

Our study demonstrated that serum AFP > 20 ng/mL and tumor-to-liver SI ratio of 0.677 or less on HBP images were significant independent variables for potentially predicting GPC3 expression in single HCC ≤ 3 cm. The diagnostic specificity of GPC3 was higher when the two variables were combined. The nomogram constructed from the prediction model was predicted satisfactorily and calibrated well in both the training and validation cohorts. Additionally, the recurrence rate in patients with GPC3-positive HCCs was significantly higher than that in patients with GPC3-negative HCCs after surgery in both cohorts.

Serum AFP > 20 ng/mL manifested as a significant factor for predicting GPC3 in the current study, which is consistent with previous studies [19, 20]. GPC3 mRNA levels in HCC were reported to be associated with serum AFP levels [21]. GPC3 and AFP may share the transcription factors such as zinc fingers and homeoboxes 2 (Zhx2) and AFP regulator 2 (Arf2), and some other tumors such as yolk sac tumors also produce AFP and GPC3 [22, 23]. In addition, previous studies have shown that AFP is related to the diagnosis and prognosis of HCC [24, 25].

The tumor-to-liver SI ratio on HBP images was significantly lower in GPC3-positive HCCs compared with GPC3-negative HCCs. Previous studies [26, 27] have shown that low tumor-to-liver SI ratio on HBP images correlates with poor histologic grade of HCC and this correlation is related to the gradual decrease of the expression of organic anion transporting polypeptide (OATP) during hepatocarcinogenesis. In addition, several reports have reported that low tumor-to-liver SI ratio on HBP images is associated with poor clinical outcomes, as these tumors have more frequent MVI and cytokeratin 19 (CK19)-positive [12, 28]. Based on these reports, we propose that GPC3-positive HCCs with low tumor-to-liver SI ratio on HBP images might have more aggressive behavior than GPC3-negative HCCs.

Tumor volume and compacity were manifested as significant factors for predicting GPC3 in univariate analysis, but not in multivariate analysis in this study. We speculate that it may be related to the insufficient sample size of the study. As a potential predictor of GPC3, 3D quantitative parameters need to be further studied and confirmed. Because, compared with some 2D morphological parameters such as tumor size, 3D quantitative analysis can provide more complete morphological information reflecting tumor heterogeneity.

The study exhibited good diagnostic performance in predicting GPC3 in HCC. The diagnostic specificity of GPC3 increased in both cohorts when combined with the two significant factors of serum AFP > 20 ng/mL and tumor-to-liver SI ratio of 0.677 or less on HBP images. The nomogram based on the prediction model performed satisfactorily in both cohorts and were well calibrated. According to the probability predicted by nomogram, patients could be stratified into high-risk group and low-risk group. For patients at low risk, not only can unnecessary medical examination or treatment be avoided, but also the burden of follow-up costs can be reduced. The nomogram might assist surgeons in treatment decision-making and facilitate personalized treatment for HCC patients.

Recurrence rates were significantly higher in patients with GPC3-positive HCCs compared with those with GPC3-negative HCCs after curative resection in both cohorts, which is consistent with previous studies [29, 30]. The evidence supports the association between GPC3 and clinical malignancy of HCC. GPC3-positive may be a significant indicator to promote the tumor inflammatory microenvironment, which in turn accelerates tumor recurrence. A previous study reported that enhanced immunoreactivity of GPC3 in HCC cells along the tumor–stromal boundary in some cases, suggesting stromal influence on GPC3 expression [29].

Our study has some limitations. First, the retrospective study design could result in selection bias. Second, the results cannot be generalized to HCC with the largest diameter greater than 3 cm, since the tumor size in the study was limited to less than 3 cm. Third, only the 3D quantitative parameters on HBP were analyzed without comparing the difference between sequences. Therefore, the results of this study need to be verified by more extensive and prospective studies.

In conclusion, serum AFP > 20 ng/mL and tumor-to-liver SI ratio of 0.677 or less on HBP images can be used as preoperative imaging biomarkers for identifying GPC3-positive small HCC. GPC3 expression is associated with recurrence after surgery of small HCC ≤ 3 cm.

Abbreviations

3D Three-dimensional

ADC Apparent diffusion coefficient

AFP Alpha-fetoprotein

AUC Area under the curve

Arf2 AFP regulator 2

CI Confidence interval

CK19 Cytokeratin 19

CT Computed tomography

DWI Diffusion-weighted imaging

GPC3 Glypican-3

HBP Hepatobiliary phase

HCC Hepatocellular carcinoma

ICC Intraclass correlation coefficients

MRI Magnetic resonance imaging

MVI Microvascular invasion

NPV Negative predictive value

OATP Organic anion-transporting polypeptide

OR Odds ratio

PACS Picture archiving and communication system

PPV Positive predictive value

ROC Receiver operating characteristic

ROI Regions of interest

SI Signal intensity

VIBE Volumetric-interpolated breath-hold examination

Zfh2 Zinc fingers and homeoboxes 2

Statements And Declarations

Funding: The authors declare that no funds, grants, or other support were received during the preparation of this manuscript.

Financial interests: The authors have no relevant financial or non-financial interests to disclose.

Author Contributions: All authors were involved in the critical revision of the manuscript. Sheng-Xiang Rao and San-Yuan Dong contributed to the study conception and design. Material preparation, data collection and analysis were performed by San-Yuan Dong, Wei Sun, Bin Xu, Wen-Tao Wang, Yu-Tao Yang and Xiao-Shan Chen. The first draft of the manuscript was written by San-Yuan Dong and all authors commented on previous versions of the manuscript. All authors read and approved the final manuscript.

References

1. Siegel RL, et al, Statistics C. 2021. CA Cancer J Clin, 2021. **71**(1): p. 7–33.
2. Rao Q, et al. Clinical benefits of PD-1/PD-L1 inhibitors in advanced hepatocellular carcinoma: a systematic review and meta-analysis. Hepatol Int. 2020;14(5):765–75.
3. Marrero JA, et al. Diagnosis, Staging, and Management of Hepatocellular Carcinoma: 2018 Practice Guidance by the American Association for the Study of Liver Diseases. Hepatology. 2018;68(2):723–50.
4. Zhang J, et al. Overexpression of glypican-3 is a predictor of poor prognosis in hepatocellular carcinoma: An updated meta-analysis. Med (Baltim). 2018;97(24):e11130.
5. Li N, et al. A Frizzled-Like Cysteine-Rich Domain in Glypican-3 Mediates Wnt Binding and Regulates Hepatocellular Carcinoma Tumor Growth in Mice. Hepatology. 2019;70(4):1231–45.
6. Gao W, et al. Inactivation of Wnt signaling by a human antibody that recognizes the heparan sulfate chains of glypican-3 for liver cancer therapy. Hepatology. 2014;60(2):576–87.
7. Fu Y, et al. Glypican-3-Specific Antibody Drug Conjugates Targeting Hepatocellular Carcinoma. Hepatology. 2019;70(2):563–76.
8. Li D, et al. Persistent Polyfunctional Chimeric Antigen Receptor T Cells That Target Glypican 3 Eliminate Orthotopic Hepatocellular Carcinomas in Mice. Gastroenterology. 2020;158(8):2250–65.e20.
9. Zhou F, et al. Glypican-3: A promising biomarker for hepatocellular carcinoma diagnosis and treatment. Med Res Rev. 2018;38(2):741–67.

10. Zech CJ, et al. Consensus report from the 8th International Forum for Liver Magnetic Resonance Imaging. Eur Radiol. 2020;30(1):370–82.
11. Lee CM, et al. Combined computed tomography and magnetic resonance imaging improves diagnosis of hepatocellular carcinoma ≤ 3.0 cm. Hepatol Int. 2021;15(3):676–84.
12. Choi SY, et al. Imaging Features of Gadoxetic Acid-enhanced and Diffusion-weighted MR Imaging for Identifying Cytokeratin 19-positive Hepatocellular Carcinoma: A Retrospective Observational Study. Radiology. 2018;286(3):897–908.
13. Hong SB, et al. MRI Features for Predicting Microvascular Invasion of Hepatocellular Carcinoma: A Systematic Review and Meta-Analysis. Liver Cancer. 2021;10(2):94–106.
14. Yamazaki M, et al. Quantitative 3D Shape Analysis of CT Images of Thymoma: A Comparison With Histological Types. AJR Am J Roentgenol. 2020;214(2):341–7.
15. Jeon SK, et al. Assessment of malignant potential in intraductal papillary mucinous neoplasms of the pancreas using MR findings and texture analysis. Eur Radiol. 2021;31(5):3394–404.
16. Dong SY, et al., Microvascular invasion of small hepatocellular carcinoma can be preoperatively predicted by the 3D quantification of MRI. Eur Radiol, 2022.
17. Dong SY, et al., Hepatobiliary phase images of gadoxetic acid-enhanced MRI may improve accuracy of predicting the size of hepatocellular carcinoma at pathology. Acta Radiol, 2021: p. 2841851211014194.
18. Yang L, et al. A Radiomics Nomogram for Preoperative Prediction of Microvascular Invasion in Hepatocellular Carcinoma. Liver Cancer. 2019;8(5):373–86.
19. Saito S, et al. Molecular background of alpha-fetoprotein in liver cancer cells as revealed by global RNA expression analysis. Cancer Sci. 2008;99(12):2402–9.
20. Gu D, et al. MRI-Based Radiomics Signature: A Potential Biomarker for Identifying Glypican 3-Positive Hepatocellular Carcinoma. J Magn Reson Imaging. 2020;52(6):1679–87.
21. Hsu HC, Cheng W, Lai PL. Cloning and expression of a developmentally regulated transcript MXR7 in hepatocellular carcinoma: biological significance and temporospatial distribution. Cancer Res. 1997;57(22):5179–84.
22. Morford LA, et al. The oncofetal gene glypican 3 is regulated in the postnatal liver by zinc fingers and homeoboxes 2 and in the regenerating liver by alpha-fetoprotein regulator 2. Hepatology. 2007;46(5):1541–7.
23. Zynger DL, et al. Expression of glypican 3 in ovarian and extragonadal germ cell tumors. Am J Clin Pathol. 2008;130(2):224–30.
24. Omata M, et al. Asia-Pacific clinical practice guidelines on the management of hepatocellular carcinoma: a 2017 update. Hepatol Int. 2017;11(4):317–70.
25. Halazun KJ, et al. Dynamic α-Fetoprotein Response and Outcomes After Liver Transplant for Hepatocellular Carcinoma. JAMA Surg. 2021;156(6):559–67.
26. Kitao A, et al. Gadoxetic acid-enhanced MR imaging for hepatocellular carcinoma: molecular and genetic background. Eur Radiol. 2020;30(6):3438–47.
27. Tsuboyama T, et al. Hepatocellular carcinoma: hepatocyte-selective enhancement at gadoxetic acid-enhanced MR imaging–correlation with expression of sinusoidal and canalicular transporters and bile accumulation. Radiology. 2010;255(3):824–33.

28. Choi JW, et al. Hepatocellular carcinoma: imaging patterns on gadoxetic acid-enhanced MR Images and their value as an imaging biomarker. Radiology. 2013;267(3):776–86.
29. Yorita K, et al. Prognostic significance of circumferential cell surface immunoreactivity of glypican-3 in hepatocellular carcinoma. Liver Int. 2011;31(1):120–31.
30. Xue R, et al. The significance of glypican-3 expression profiling in the tumor cellular origin theoretical system for hepatocellular carcinoma progression. J Gastroenterol Hepatol. 2017;32(8):1503–11.

Tables

Table 1. Patient Characteristics

Variable	Training cohort (n = 117)			Validation cohort (n = 32)			P Value
	GPC3 (+) 84	GPC3 (-) 33	P Value	GPC3 (+) 22	GPC3 (-) 10	P Value	0.736
Age (years)*	53.3 ± 11.1	59.4 ± 11.4	0.009	52.5 ± 9.8	58.8 ± 12.0	0.124	0.786
Gender			0.721			0.387	0.457
Male	71 (84.5)	27 (81.8)		16 (72.7)	9 (90.0)		
Female	13 (15.5)	6 (18.2)		6 (27.3)	1 (10.0)		
Intrahepatic location			0.364			0.106	0.086
Right	66 (78.6)	27 (81.8)		12 (54.5)	9 (90.0)		
Left	15 (17.9)	6 (18.2)		10 (45.5)	1 (10.0)		
Caudate lobe or border area	3 (3.5)	0 (0)		0 (0)	0 (0)		
			0.706			0.712	0.089
Background liver tissue	59 (70.2)	22 (66.7)		11 (50.0)	6 (60.0)		
Liver cirrhosis	25 (29.8)	11 (33.3)		11 (50.0)	4 (40.0)		
None			0.496			0.534	1.000
Etiology of liver disease	79 (94.0)	29 (88.0)		21 (95.5)	9 (90.0)		
Hepatitis B virus	2 (2.4)	1 (3.0)		1 (4.5)	1 (10.0)		
Hepatitis C virus	3 (3.6)	3 (9.0)		0 (0)	0 (0)		
None or other			0.001			0.712	0.613
Edmondson-Steiner grade	41 (48.8)	27 (81.8)		11 (50.0)	6 (60.0)		
G1-G2	43 (51.2)	6 (18.2)		11 (50.0)	4 (40.0)		
G3-G4			0.278			1.000	1.000
	9 (10.7)	1 (3.0)		2 (9.1)	0 (0)		
Satellite nodule	75 (89.3)	32 (97.0)		20 (90.9)	10 (100.0)		
Presence			0.001			0.022	0.637
Absence	37 (44.0)	27 (81.8)		8 (36.4)	8 (80.0)		
Serum AFP	47 (56.0)	6 (18.2)		14 (63.6)	2 (20.0)		
≤ 20 ng/mL			0.274			1.000	0.191
> 20 ng/mL	77 (91.7)	28 (84.8)		18 (81.8)	8 (80.0)		
Total bilirubin	7 (8.3)	5 (15.2)		4 (18.2)	2 (20.0)		
≤ 20.4 μmol/L			0.018			0.210	0.234
> 20.4 μmol/L	25 (29.8)	3 (9.1)		6 (27.3)	5 (50.0)		

Microvascular invasion	59 (70.2)	30 (90.9)	16 (72.7)	5 (50.0)
Presence				
Absence				

* Data are continuous variables, reported as means ± standard deviations.

Unless otherwise indicated, data are number of patients, with percentage in parentheses. *AFP* alpha-fetoprotein, *GPC3* Glypican-3

Table 2. Quantitative MR Imaging Findings

Variable	Training cohort (n = 117)				Validation cohort (n = 32)				P Value
	GPC3 (+) 84	GPC3 (-) 33	P Value	ICC	GPC3 (+)	GPC3 (-)	P Value	ICC	0.736
Volume (mL)	3.184 (0.934, 4.824)	2.015 (0.557, 3.132)	0.031	0.996	3.749 (1.922, 7.854)	3.437 (1.614, 7.673)	0.087	0.997	0.100
Sphericity	0.804 (0.764, 0.824)	0.814 (0.781, 0.831)	0.203	0.908	0.777 (0.764, 0.815)	0.773 (0.732, 0.819)	0.515	0.975	0.390
Compacity	2.000 (1.591, 2.726)	1.715 (1.403, 2.226)	0.034	0.936	2.338 (1.917, 3.157)	2.431 (1.833, 3.120)	0.935	0.998	0.060
ADC Value	1.178 (0.938, 1.456)	1.225 (1.018, 1.490)	0.531	0.995	1.181 (1.036, 1.349)	1.199 (0.905, 1.304)	0.684	0.986	0.877
Tumor size (cm)	1.650 (1.225, 2.300)	1.500 (1.200, 1.750)	0.062	0.975	2.100 (1.375, 2.800)	2.000 (1.475, 2.000)	0.790	0.992	0.150
Tumor-to-liver SI ratio on DWI	1.691 (1.389, 2.116)	1.525 (1.340, 1.784)	0.031	0.998	1.666 (1.317, 1.861)	1.602 (1.248, 2.072)	0.776	0.995	0.497
Tumor-to-liver SI ratio on HBP	0.560 (0.475, 0.643)	0.688 (0.561, 0.800)	<0.001	0.996	0.473 (0.417, 0.628)	0.535 (0.490, 0.663)	0.038	0.942	0.410

Data are median (interquartile range).

ADC apparent diffusion coefficient, *SI* signal intensity, *DWI* diffusion-weighed imaging, *HBP* hepatobiliary phase, *GPC3* Glypican-3, *ICC* intraclass correlation coefficients

Table 3. Qualitative MR Imaging Findings

Variable	Training cohort (n = 117)				Validation cohort (n = 32)				P Value
	GPC3 (+)	GPC3 (-)	P Value	kappa	GPC3 (+)	GPC3 (-)	P Value	kappa	0.736
Arterial rim enhancement			0.482	0.862			0.637	0.904	0.558
Presence	11 (13.1)	6 (18.2)			5 (22.7)	1 (10.0)			
Absence	73 (86.9)	27 (81.8)	0.100	0.906	17 (77.3)	9 (90.0)	0.811	0.938	0.063
Arterial peritumoral enhancement									
Presence	34 (40.5)	8 (24.2)			12 (54.5)	5 (50.0)			
Absence	50 (59.5)	25 (75.8)	0.015	0.912	10 (45.5)	5 (50.0)	0.252	0.875	0.412
Tumor margin									
Non-smooth	41 (48.8)	8 (24.2)	0.386	0.892	13 (59.1)	3 (30.0)	0.703	0.867	0.060
Smooth	43 (51.2)	25 (75.8)			9 (40.9)	7 (70.0)			
Tumor capsule			0.078	0.796			1.000	1.000	1.000
Complete	65 (77.4)	23 (70.0)			13 (59.1)	7 (70.0)			
Incomplete or absent	19 (22.6)	10 (30.0)	0.472	0.897	9 (40.9)	3 (30.0)	1.000	0.870	0.130
Tumor hypointensity on HBP									
Presence	84 (100.0)	31 (93.9)			22 (100.0)	10 (100.0)			
Absence	0 (0)	2 (6.1)	0.317	0.902	0 (0)	0 (0)	0.547	0.940	0.149
Peritumoral hypointensity on HBP									
Presence	26 (31.0)	8 (24.2)			9 (40.9)	4 (40.0)			
Absence	58 (69.0)	25 (75.8)			13 (59.1)	6 (60.0)			
Enhancement pattern									
Arterial enhancement with washout	70 (83.3)	25 (75.7)			19 (86.5)	7 (70.0)			
No or minimal enhancement	7 (8.3)	2 (6.1)			2 (9.0)	2 (20.0)			
Persistent enhancement	6 (7.1)	6 (18.2)			1 (4.5)	1 (10.0)			
	1 (1.3)				0 (0)	0 (0)			

Progressive enhancement	0 (0)

Data are number of patients, with percentage in parentheses.

HBP hepatobiliary phase, *GPC3* Glypican-3

Table 4. Univariate and Multivariate Analyses in Prediction of GPC3-positive HCC in the Training Cohort

Variable	Univariate Analysis		Multivariate Analysis	
	Odds Ratio (95% CI)	P Value	Odds Ratio (95% CI)	P Value
Age (years)	0.950 (0.912-0.989)	0.012	0.956 (0.910-1.005)	0.081
Serum AFP > 20 ng/mL	5.716 (2.137-15.290)	0.001	5.215 (1.701-15.991)	**0.004***
Volume (mL)	1.201 (0.998-1.445)	0.053	1.132 (0.608-2.108)	0.696
Compacity	1.978 (1.031-3.797)	0.040	1.601 (1.157-16.293)	0.691
Tumor-to-liver SI ratio on DWI	2.144 (0.938-4.898)	0.070	1.332 (0.521-3.404)	0.549
Tumor-to-liver SI ratio on HBP	0.001 (0.000-0.040)	<0.001	0.003 (0.000-0.175)	**0.005***
Non-smooth tumor margin	2.980 (1.207-7.357)	0.018	2.160 (0.704-0.175)	6.628

The asterisk indicates statistical signifcance

AFP alpha-fetoprotein, *SI* signal intensity, *DWI* diffusion–weighted imaging, *HBP* hepatobiliary phase, *GPC3* Glypican-3, *HCC* hepatocellular carcinoma, *CI* confidence interval

Table 5. Diagnostic Performance of Significant Imaging Findings and Combination for Predicting GPC3-positive HCC

Variable	Sensitivity	Specificity	Accuracy	PPV	NPV
Training Cohort					
Serum AFP > 20 ng/mL	56.0(47/84)	81.8(27/33)	63.2(74/117)	88.7(47/53)	42.2(27/64)
Tumor-to-liver SI ratio on HBP < 0.677	88.1(74/84)	54.5(18/33)	78.6(92/117)	83.1(74/89)	64.3(18/28)
Combination of the two findings	51.2(43/84)	87.9(29/33)	61.5(72/117)	91.5(43/47)	41.4(29/70)
Validation Cohort	63.6(14/22)	80.0(8/10)	68.8(22/32)	87.5(14/16)	50.0(8/16)
Serum AFP > 20 ng/mL	86.3(19/22)	30.0(3/10)	68.8(22/32)	73.1(19/26)	50.0(3/6)
Tumor-to-liver SI ratio on HBP < 0.677	50.0(11/22)	90.0(9/10)	62.5(20/32)	91.7(11/12)	45.0(9/20)
Combination of the two findings					

Data are presented as percentages. Data in parentheses are the number of subjects used to calculate the percentage.

AFP alpha-fetoprotein, *SI* signal intensity, *HBP* hepatobiliary phase, *GPC3* Glypican-3, *HCC* hepatocellular carcinoma, *PPV* positive predictive value, *NPV* negative predictive value

Figures

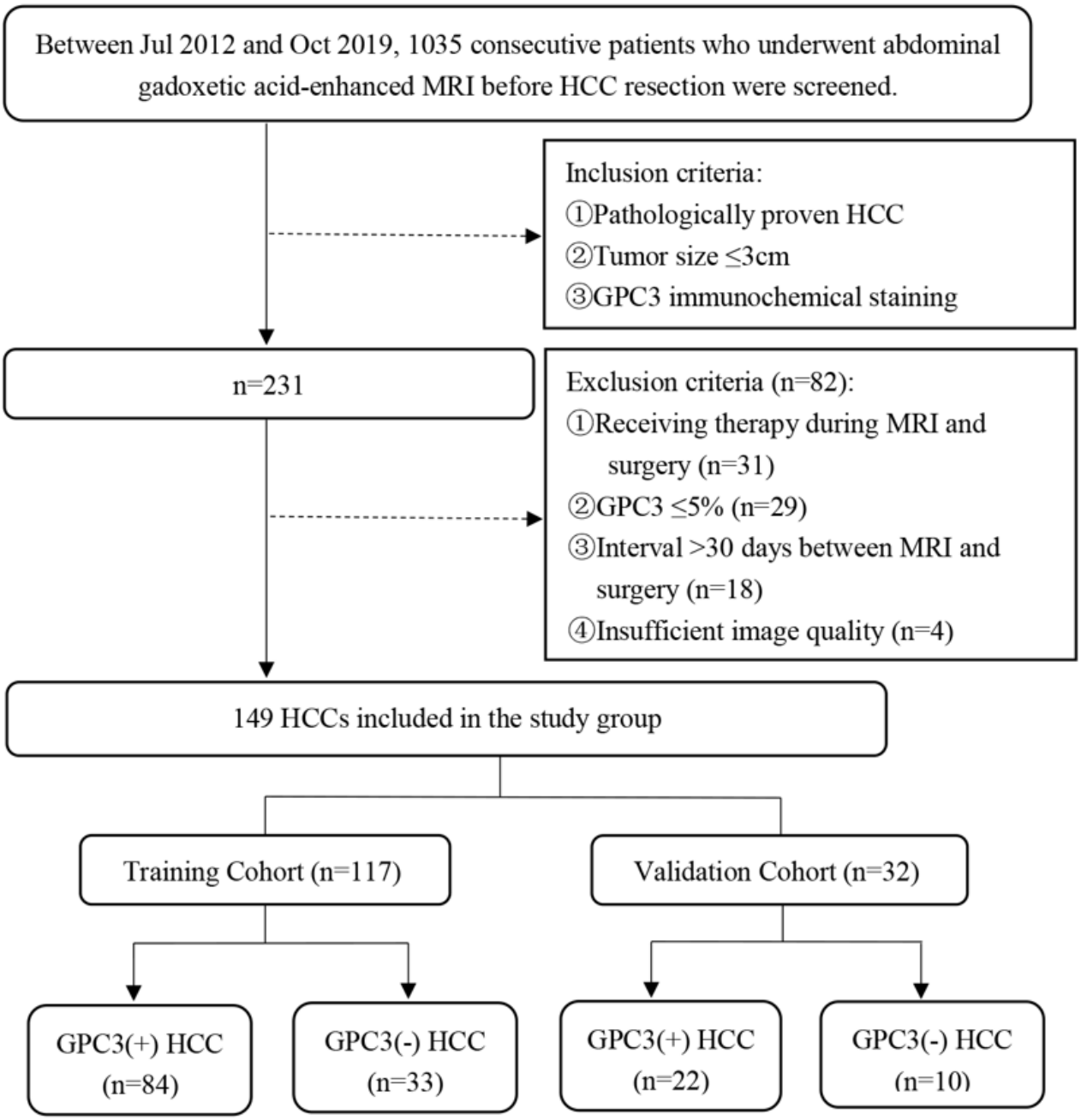

Figure 1

Flow diagram shows inclusion and exclusion criteria for the study

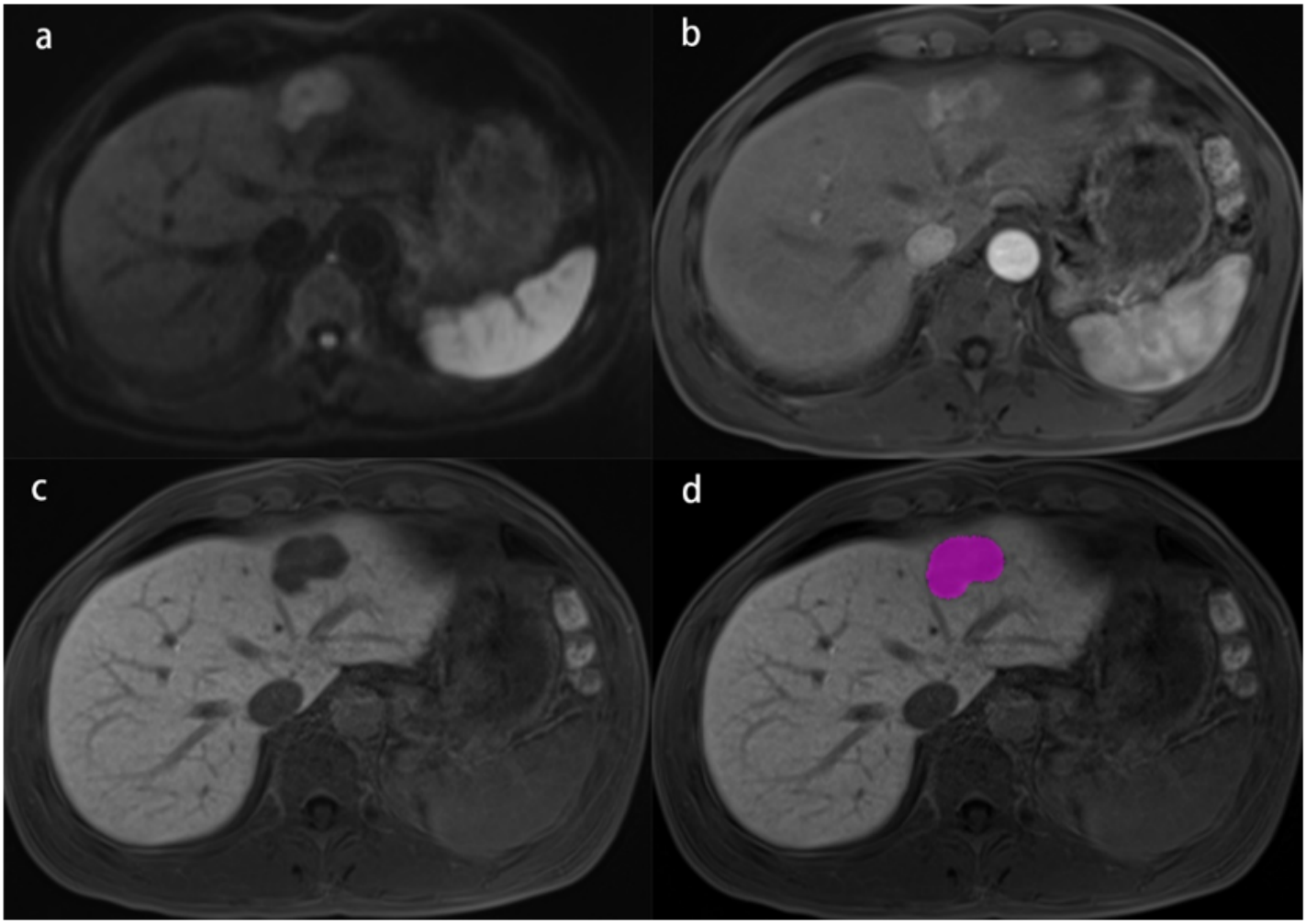

Figure 2

Gadoxetic acid–enhanced MR images of a 51-year-old male patient with pathologically verified GPC3-positive HCC. (**a**) Diffusion-weighted imaging shows a 3.0-cm hyperintense mass in the left hepatic lobe, and the tumor-to-liver SI ratio is 1.584. (**b**) The arterial phase shows heterogeneous enhancement of the lesion. (**c**) The hepatobiliary phase image shows that the lesion is hypointense with a non-smooth margin, and the tumor-to-liver SI ratio is 0.349. (**d**) The lesion was segmented on the hepatobiliary phase image and recurrence occurred in the liver 12 months after surgery.

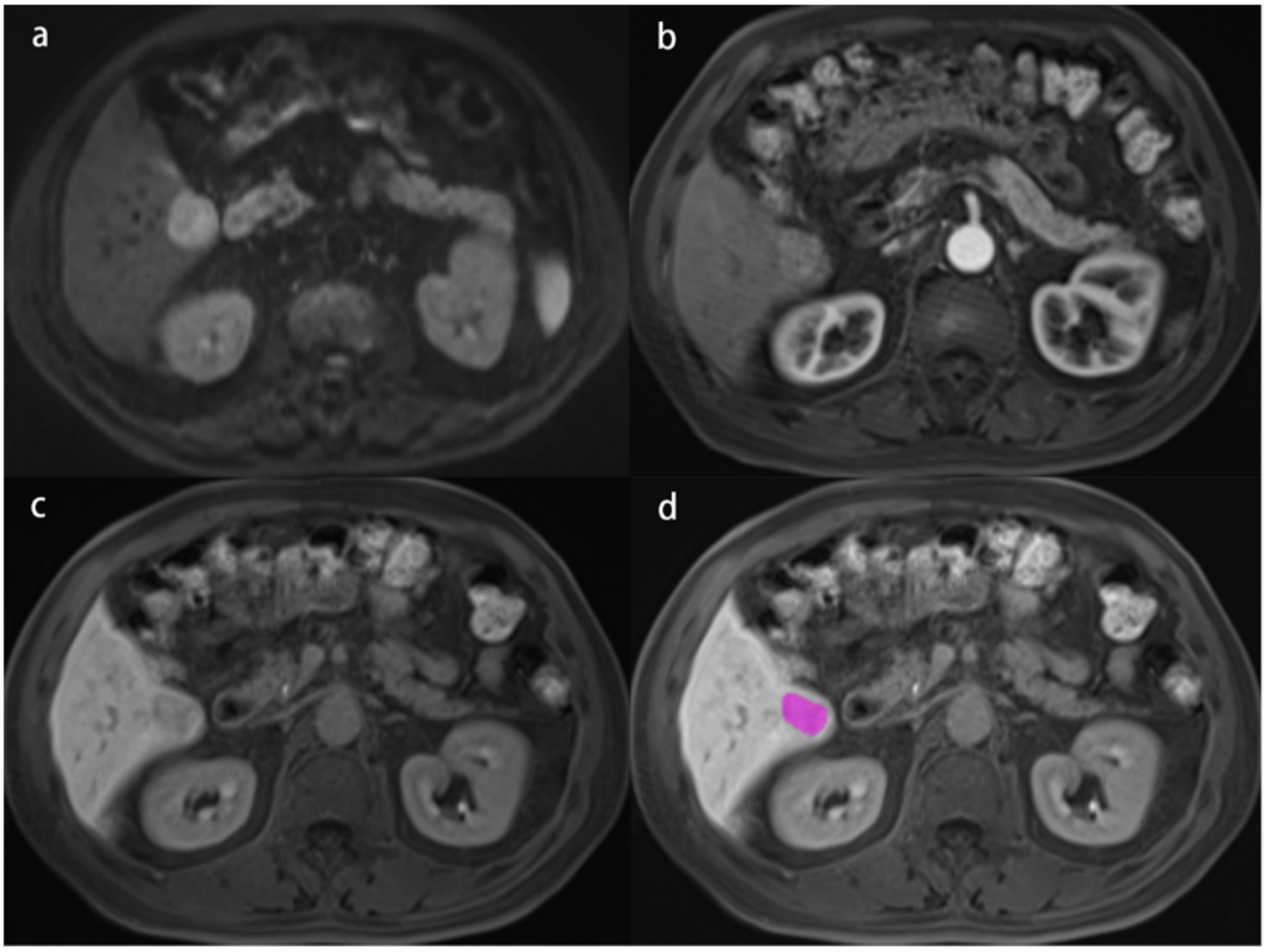

Figure 3

Gadoxetic acid–enhanced MR images of a 74-year-old male patient with pathologically verified GPC3-negative HCC. (**a**) Diffusion-weighted imaging shows a 2.8-cm hyperintense mass in the left hepatic lobe, and the tumor-to-liver SI ratio is 2.25. (**b**) The arterial phase shows heterogeneous enhancement of the lesion. (**c**) The hepatobiliary phase image shows that the lesion is hypointense with a smooth margin, and the tumor-to-liver SI ratio is 0.839. (**d**) The lesion was segmented on the hepatobiliary phase image and did not recur during the 36 months follow-up period after surgery.

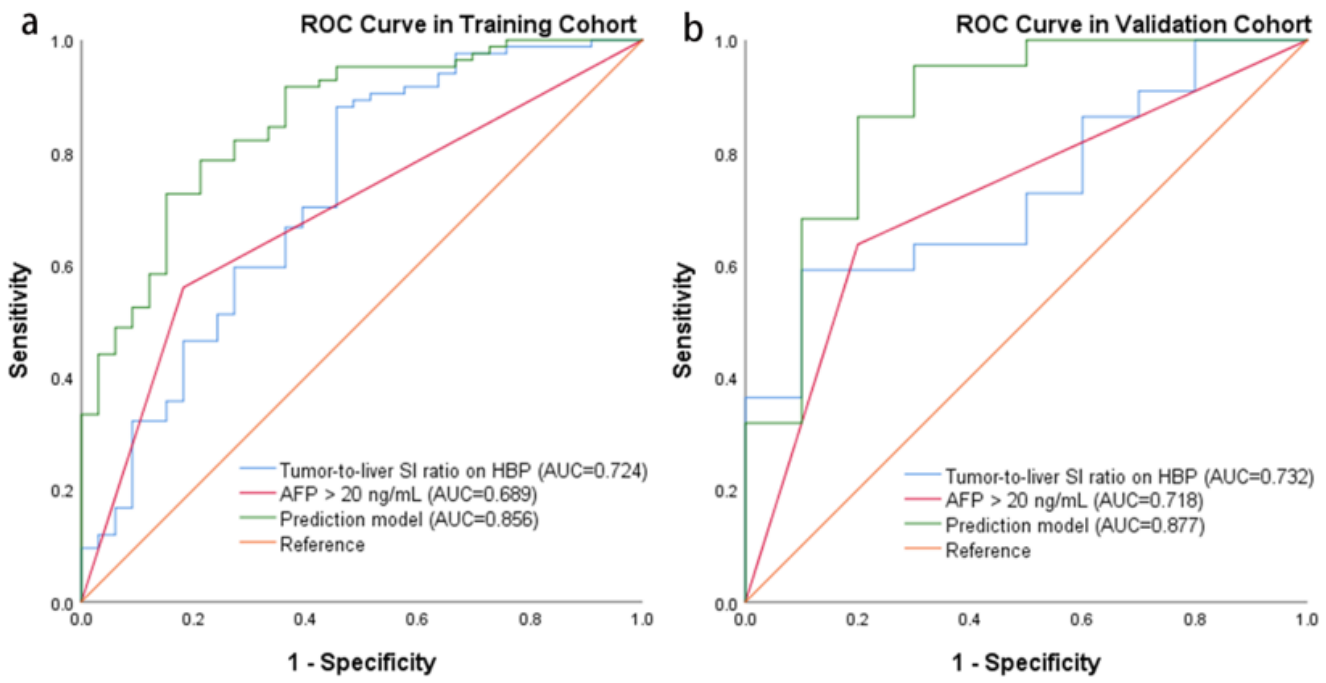

Figure 4

Receiver operating characteristic (ROC) curve of the two significant MR imaging findings and diagnostic model in the prediction of GPC3 expression for small hepatocellular carcinomas (**a**) ROC curve in the training cohort; (**b**) ROC curve in the validation cohort. *AUC* area under the curve, *SI* signal intensity, *HBP* hepatobiliary phase, *AFP* alpha-fetoprotein

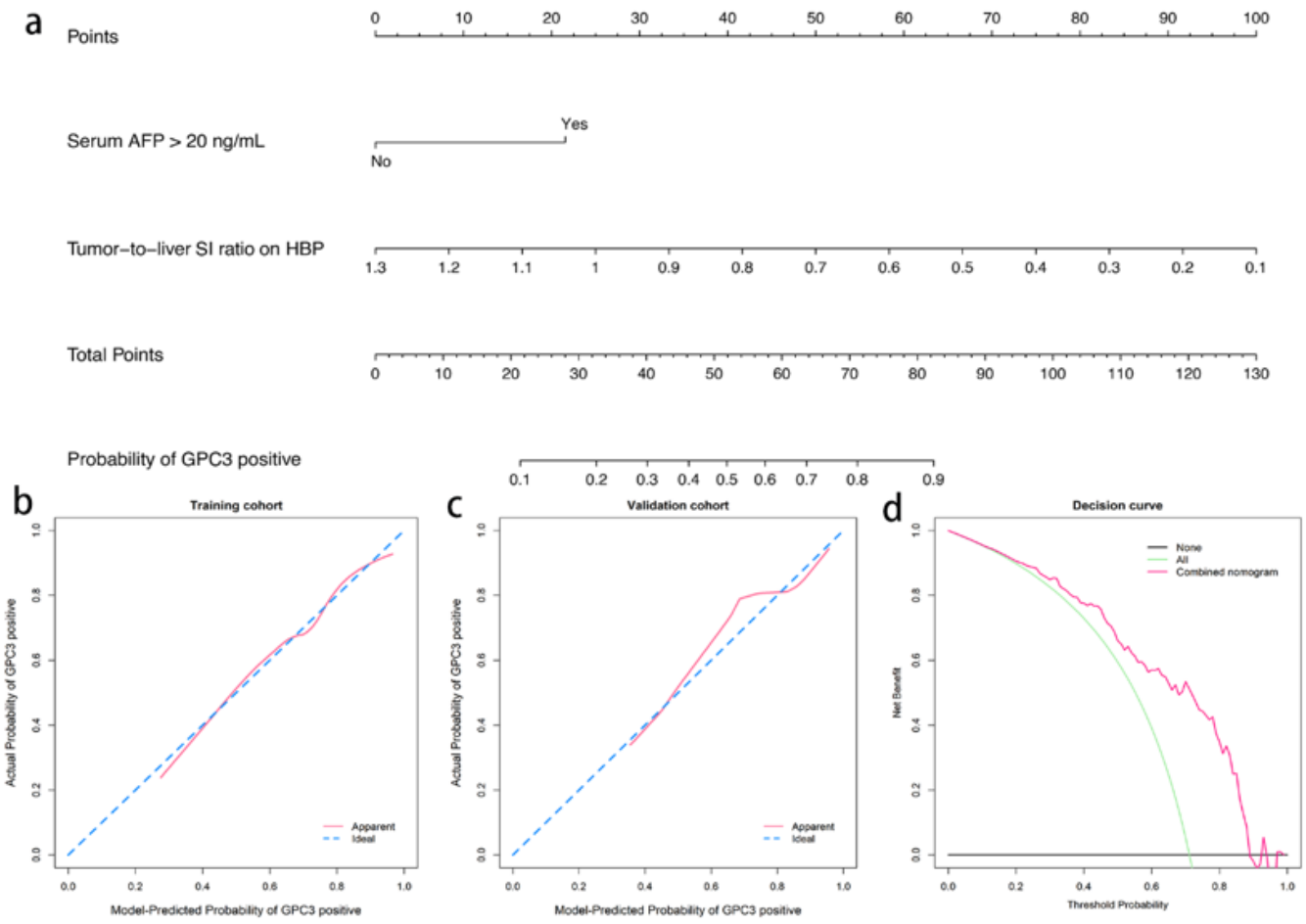

Figure 5

Nomogram for Preoperative Estimation of GPC3 Risk and Its Predictive Performance (**a**) Nomogram for predicting GPC3-positive probabilities, which integrated the two significant MR imaging findings: serum AFP > 20 ng/mL and tumor-to-liver SI ratio on HBP. The prediction point is located on the uppermost point scale corresponding to each variable. On the bottom scale, the points of all variables are added up and converted into the GPC3-positive probability. (**b-c**) Calibration curves of the nomogram in the training and validation cohorts. X-axis is nomogram predicted probability of GPC3-positive; Y-axis is observed GPC3-positive, and the diagonal dashed line represents the ideal prediction by a perfect model. (**d**) Decision curves of the nomogram in the whole cohort. The green line is the net benefit of assuming that all patients have GPC3-positive; the black line is the net benefit of assuming no patients have GPC3-positive; and the red line is expected net benefit of per patient based on the predictive nomogram.

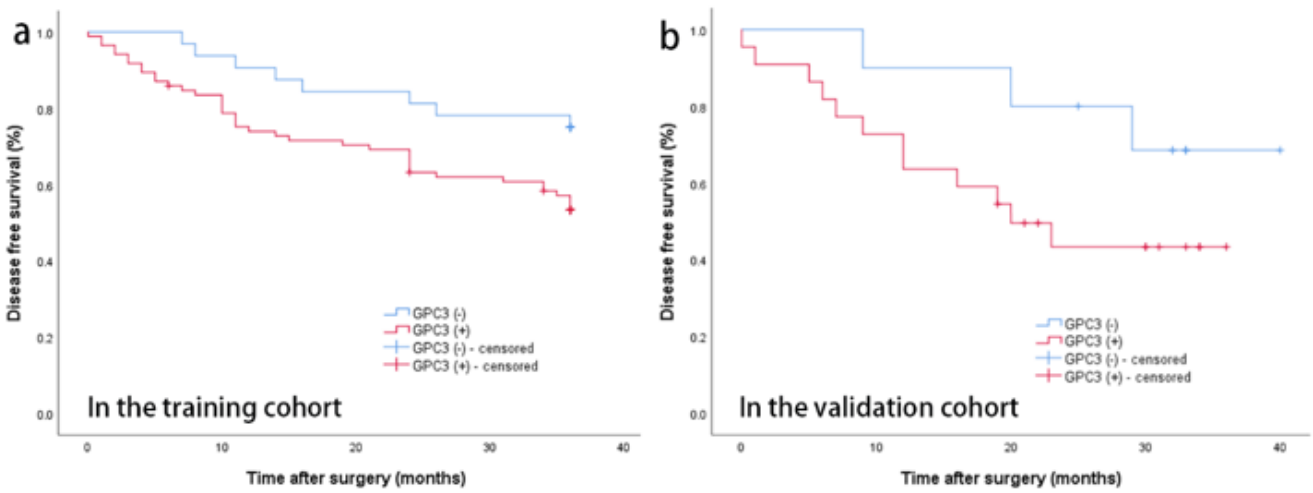

Figure 6

Recurrence rates of patients (**a**) In the training cohort; (**b**) In the validation cohort.

Supplementary Files

This is a list of supplementary files associated with this preprint. Click to download.

- SupplementaryMaterial.docx